Chiral Ordering and Conformational Dynamics for a Class of Oligo-phenylene-ethynylenes on Au(111)

Carsten Busse,[†] Sigrid Weigelt, Lars Petersen, Erik Lægsgaard, Flemming Besenbacher, and Trolle R. Linderoth*

Interdisciplinary Nanoscience Center, iNANO, University of Aarhus, DK-8000 Aarhus C, Denmark, and Department of Physics and Astronomy, University of Aarhus, DK-8000 Aarhus C, Denmark

Anne H. Thomsen, Morten Nielsen, and Kurt V. Gothelf

Interdisciplinary Nanoscience Center, iNANO, University of Aarhus, DK-8000 Aarhus C, Denmark, and Department of Chemistry, University of Aarhus, DK-8000 Aarhus C, Denmark

Received: January 30, 2007; In Final Form: March 27, 2007

Adsorption structures formed from a class of planar organic molecules on the Au(111) surface under ultrahigh vacuum conditions have been characterized using scanning tunneling microscopy (STM). The molecules have different geometries, linear, bent, or three-spoke, but all consist of a conjugated aromatic backbone formed from three or four benzene rings connected by ethynylene spokes and functionalized at all ends with an aldehyde, a hydroxyl, and a bulky *tert*-butyl group. Upon adsorption, the molecules adopt different surface conformations some of which are chiral. For the majority of the observed adsorption structures, chirality is expressed also in the molecular tiling pattern, and the two levels of chirality display a high degree of correlation. The formation and chiral ordering of the self-assembled structures are shown to result from dynamic interchanges between a diffusing lattice gas and the nucleated islands, as well as from a chiral switching process in which molecules alter their conformation by an intramolecular rotation around a molecular spoke, enabling them to accommodate to the tiling pattern of the surrounding molecular structures. The kinetics of the conformational switching is investigated from time-resolved, variable temperature STM, showing the process to involve an activation energy of ∼0.3 eV depending on the local molecular environment. The molecule−molecule interactions appear primarily to be of van der Waals character, despite the investigated compounds having functional moieties capable of forming intermolecular hydrogen bonds.

I. Introduction

Molecular nanostructures[1] on solid surfaces formed by spontaneous bottom-up self-assembly[2] are central to future nanotechnology and will be essential to fields such as surface functionalization, bio-sensors, molecular electronics, or heterogeneous asymmetric catalysis. To control, and ultimately exploit, molecular self-assembly on surfaces, a detailed understanding of intermolecular interactions and molecular dynamical processes is required, and a range of systems of increasing size and complexity have over the last years been investigated, in particular, by the technique of scanning tunneling microscopy (STM). Self-assembly of organic molecules on surfaces is based on spontaneous aggregation steered by noncovalent interactions such as hydrogen bonds,[3−7] van der Waals interactions,[8] dipole−dipole interactions,[9−11] or metal−ligand complexation.[5,12] Formation of specific nano-architectures on surfaces has been achieved by controlling both the geometry[13] and the functional groups[9] of the molecular building blocks. Using time-resolved STM, dynamic processes involved in the formation of molecular structures have been investigated, such as diffusion[14−18] and rotation[12,18−20] of individual molecules as well as equilibrium exchange between a lattice gas of diffusing molecules and condensed molecular aggregates.[21] Intramolecular conformational degrees of freedom are also of high importance in self-assembly processes, but studies into this have mainly focused on the identification[22] or manipulation[23−25] of molecular conformation by STM while less focus has been on elucidating the dynamics of spontaneous conformational changes.[26,27]

Molecular adsorption systems often display pronounced stereochemical effects.[28,29] The most obvious case arises if chiral molecules, that is, molecules without an inversion symmetry element, are deposited onto a surface. In this case, the chirality of the adsorbate is transferred to the adsorption system, and STM has been used to identify and investigate chiral effects in several such cases.[30−34] At another extreme, surface chirality can arise even for highly symmetric adsorbates provided they adsorb in such a way that the molecule−surface system in combination does not have any mirror symmetry elements.[35] An intermediate case occurs for molecules that are achiral in the gas phase but become chiral once adsorbed because the confinement in two dimensions removes mirror symmetry in the plane of the substrate.[36−39] Such compounds are said to be prochiral, and their adsorption will always lead to equal amounts of mirror-image surface enantiomers. Often, such adsorption systems display phase separation into homochiral domains. It has in general been believed that the confinement on the surface would be sufficiently strong to render the chiral sense of an individual prochiral molecule irreversibly fixed upon adsorption,

* Corresponding author. E-mail: trolle@inano.dk. Phone: +45 8942 5536. Fax: +45 8942 3690.

[†] Present address: II. Physikalisches Institut, Universität zu Köln, D-50937 Köln, Germany.

10.1021/jp0707891 CCC: $37.00
Published on Web 05/09/2007

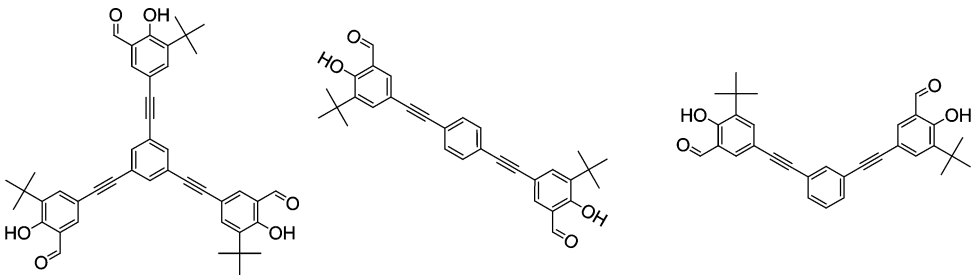

Figure 1. Three compounds studied here with (from left to right) three-spoke, para, and meta configuration.

and phase separation has therefore been ascribed to lateral mass transport in combination with intermolecular chiral recognition at domain boundaries.[36]

In this work, we investigate chiral ordering and conformational dynamics for a class of three conjugated organic molecules (oligo-phenylene-ethynylenes) using time-resolved STM under ultrahigh vacuum (UHV) conditions (see Figure 1). The molecules vary in geometry but contain the same functional moieties. After adsorption on a Au(111) surface, the molecules assume various surface conformations, some of which are chiral. Chirality is also expressed in the tiling pattern of several of the observed molecular adsorption structures, and we find that the two levels of chirality, organizational and intramolecular, display a high degree of correlation which, for some of the structures, reflects differences in interaction energies between different surface conformers as small as 0.005−0.05 eV. Dynamically, the molecules are found to be able to undergo a thermally induced conformational change, involving rotation of a bulky molecular end group, which causes them to switch between chiral and nonchiral forms or between opposite surface enantiomers. Kinetic studies performed in the temperature interval 150−220 K show the conformational switching to occur with an activation energy of approximately 0.3 eV. The observed chiral switching enables a new mechanism toward segregation into homochiral domains in which the molecules dynamically accommodate to the chirality of the surrounding tiling pattern. This new mechanism offers perspectives with respect to forming homochiral surface assemblies by seeding[35,40] with a small quantity of an appropriate chiral compound. Parts of this work were presented previously in letter form[41] (see also ref 42), focusing on one of the investigated molecules. In the present paper, we provide a significant extension of this study by showing the switching phenomenon to be general for this entire class of compounds and also provide more details on experiments and analysis.

II. Methods

A. Experimental Details. The experiments were performed in a UHV chamber equipped with standard facilities for sample preparation and characterization as well as the home-built, variable temperature Aarhus scanning tunneling microscope.[43,44] An atomically clean Au(111) single-crystal surface was prepared by repeated cycles of sputtering with 1.5 keV Ar^+ ions followed by annealing to 840−900 K, resulting in a well-ordered herringbone ($22 \times \sqrt{3}$) reconstruction.[45] The molecules, which form a solid at room temperature, were ground into a powder and evaporated in situ from a glass crucible surrounded by a thin metal wire for resistive heating. The crucible temperature was monitored with a NiCr/Ni thermocouple pair melted into the glass. The three molecules were sublimated at specific temperatures in the range 360−400 K. Prior to evaporation, the powder was thoroughly out-gassed at the deposition temperature followed by a brief heating to a slightly higher temperature. The molecules were deposited in submonolayer coverage onto a Au sample held at approximately 300 K. Prior to imaging, the substrate was cooled to lower temperatures in the STM. Temperatures of 140−170 K were applied unless clearly stated otherwise. Close-packed self-assembled molecular islands of monomolecular height were observed for all compounds investigated in this study. In general, the molecules were best imaged at ≈1 V bias voltage and ≈1 nA tunneling current. The polarity of the bias voltage did not have any systematic influence on the appearance of the molecules in the STM images, but negative bias voltage (applied to the sample) typically resulted in a more stable tunneling junction.

B. Analysis. *1. Unit Cells.* The unit cell of the observed molecular structure is defined by $|\vec{a}_o|$, $|\vec{b}_o|$, the angle between $\vec{b}_o$ and $\vec{a}_o$, and the angle between $\vec{b}_o$ and the closest ⟨110⟩ direction; see Table 1. The uncertainty in the measured angles and distances is estimated to be less than 5% resulting from dynamic distortions of the image caused by thermal drift and piezo creep and resulting from static distortions caused by anisotropies in the scanner tube. Consequently, the STM data alone does not allow us to unambiguously determine whether an overlayer is commensurate or incommensurate. The unit cell vectors were determined from the STM data and approximated by integer−value vectors.[29]

$$\begin{pmatrix} \vec{a}_o \\ \vec{b}_o \end{pmatrix} = M \begin{pmatrix} \vec{a}_s \\ \vec{b}_s \end{pmatrix} \tag{1}$$

(The contraction of the Au lattice by 4% along one close-packed direction because of the herringbone reconstruction does not seem to affect the adsorption structures and is neglected.)

As a measure for the molecular packing density, we use A_{vdW}/A_{mol}, where A_{mol} is the area occupied by one molecule in the overlayer (A_{mol} = area of unit cell/N, where N is the number of molecules in the unit cell) and A_{vdW} is the projected van der Waals area[46] (compare Figure 4a,d,g; $A_{vdW} = 274$ Å^2 for the three-spoke and 185 Å^2 for the two-spoke compounds, assuming the whole conjugated system to be parallel to the surface).

2. Switching Rates. In section IVC, we show that the investigated molecules undergo conformational switching after adsorption by intramolecular rotations (see Figure 10b−d). In particular, the switching[41] between head-to-head trans and cis arrangements (see section IIIC1) in the brick wall structure for the para compound was investigated in detail. In this section, we will show how the switching rates from trans-to-cis (cis-to-trans) states, Γ_{t-c} (Γ_{c-t}), can be connected to measurable data from time-resolved STM movies by solving a set of coupled differential equations. The input STM data directly determined from the STM movies are the time between two consecutive

TABLE 1: Overview of the Experimental Results of All Adsorption Structures[a]

compound	structure	$\lvert\vec{a}_o\rvert$ [Å]	$\lvert\vec{b}_o\rvert$ [Å]	$\angle\vec{b}_o,\vec{a}_o$ [deg]	$\angle\vec{b}_o$, ⟨110⟩ [deg]	N	A_{mol} [Å^2]	A_{vdW}/A_{mol}	matrix
para	brick wall	30	25	143	−23	2	230	0.80	$\begin{pmatrix} 3 & -9 \\ 4 & 10 \end{pmatrix}$
	grid	26	36	135	−15	2	320	0.58	$\begin{pmatrix} 5 & -5 \\ 4 & 14 \end{pmatrix}$
meta		30	29	88	−30	4	220	0.85	$\begin{pmatrix} 10 & 0 \\ 6 & 12 \end{pmatrix}$
three-spoke	hexagonal	27	26	120	19	2	310	0.88	$\begin{pmatrix} 11 & 4 \\ -4 & 7 \end{pmatrix}$
	row	28	32	92	−3	2	440	0.63	$\begin{pmatrix} 11 & 4 \\ 1 & 11 \end{pmatrix}$
	dense ladder	30	23	128	−5.0	2	260	0.96	$\begin{pmatrix} 10 & -2 \\ 0 & 8 \end{pmatrix}$
	open ladder	39	24	125	0	2	390	0.70	$\begin{pmatrix} 13 & -1 \\ 0 & 8 \end{pmatrix}$

[a] $\lvert\vec{a}_o\rvert$, $\lvert\vec{b}_o\rvert$: length of unit cell vectors as defined in Figures 5, 6, 7, and 8. $\angle\vec{b}_o,\vec{a}_o$: angle between the lattice vectors. $\angle\vec{b}_o$, ⟨110⟩: angle between $\vec{b}_o$ and the closest ⟨110⟩ direction. n: number of molecules per unit cell. A_{mol}: area occupied by one molecule. A_{vdW}/A_{mol}: packing density. Matrix: best fit to the superstructure assuming commensurability; see Methods. The uncertainties in distances and angles are ≈5%.

images, the number of flips N_{c-t} (N_{t-c}) that change cis pairs to trans pairs (trans pairs to cis pairs) between two consecutive images, and the population, $N_c(0)$ ($N_t(0)$), of cis (trans) pairs counted in the first image.

The change in the number of cis pairs (trans pairs), dN_c (dN_t), in a short time interval is given by:

$$dN_{c(t)} = -\Gamma_{c-t(t-c)}N_{c(t)}\,dt + \Gamma_{t-c(c-t)}N_{t(c)}\,dt \qquad (2)$$

where $N = N_t + N_c$ is the total number of pairs, and N_c (N_t) is the number of pairs in a cis (trans) configuration. The solutions consist of a steady-state and an exponentially decaying term:

$$N_{t(c)}(t) = \left(N_{t(c)}(0) - \frac{\Gamma_{c-t(t-c)}}{\Gamma_{c-t}+\Gamma_{t-c}}N\right)e^{-(\Gamma_{c-t}+\Gamma_{t-c})t} + \frac{\Gamma_{c-t(t-c)}}{\Gamma_{c-t}+\Gamma_{t-c}}N \qquad (3)$$

If only the population of trans pairs in an image is considered (i.e., $N = N_t(0)$, $N_c(0) = 0$), the above solutions give the number of trans pairs that have converted to cis pairs, N_{t-c}, after the time t at given switching rates. By symmetry, we can find the number of cis pairs that during time t will be changed to trans pairs, N_{c-t}, by considering the original population of cis pairs (i.e., $N = N_c(0)$, $N_t(0) = 0$):

$$N_{t-c(c-t)}(t) = -\frac{\Gamma_{t-c(c-t)}}{\Gamma_{t-c}+\Gamma_{c-t}}N_{t(c)}(0)\,e^{-(\Gamma_{t-c}+\Gamma_{c-t})t} + \frac{\Gamma_{t-c(c-t)}}{\Gamma_{t-c}+\Gamma_{c-t}}N_{t(c)}(0) \qquad (4)$$

From eq 4, we can find the corresponding switching rates, Γ_{t-c} and Γ_{c-t}:

$$\Gamma_{t-c(c-t)} = -\frac{N_{t-c(c-t)}}{N_{t(c)}(0)}\frac{\ln(1-(N_{c-t}/N_c(0))-(N_{t-c}/N_t(0)))}{((N_{c-t}/N_c(0))+(N_{t-c}/N_t(0)))t} \qquad (5)$$

The above deduction of the flipping rates from coupled differential equations takes into account the occurrence of multiple flips and areas with a nonequilibrium cis/trans population observed in the movies.

C. Organic Synthesis. *1. General Conditions.* Standard Schlenk and vacuum line techniques were employed using argon as the inert atmosphere for all manipulations of air- or moisture-sensitive compounds. Commercially available starting materials were used without further purification. Solvents were dried according to standard procedures. Purification of the products was carried out by flash chromatography (FC) using Merck silica gel 60 (230−400 mesh). ^{1}H and ^{13}C NMR spectra were recorded at 400 and 100 MHz, respectively, using $CDCl_3$ as the solvent and were reported in parts per million downfield from tetramethylsilane (TMS) ($\delta = 0$) for ^{1}H NMR and relative to the central $CDCl_3$ resonance ($\delta = 77.00$) for ^{13}C NMR. Mass spectra and high-resolution mass spectra were obtained on an liquid chromatography time-of-flight (LC-TOF) spectrometer (Micromass). Triethylamine was distilled from CaH_2 under argon prior to use. Bis(triphenylphosphine)palladium(II) chloride (Aldrich) was purchased from commercial sources. 1,3-Diethynylbenzene[47] was synthesized according to literature procedures.

The three-spoke molecule (1,3,5-tris[5-*tert*-butyl-3-formyl-4-hydroxyphenyl)ethynyl]benzene)[48,49] and the para compound (1,4-bis[5-*tert*-butyl-3-formyl-4-hydroxyphenyl)ethynyl]benzene)[49,50] were prepared according to previously described procedures.

2. 1,3-Bis[(5-tert-butyl-3-formyl-4-hydroxyphenyl)ethynyl]-benzene (Meta Compound). Bis(triphenylphosphine)palladium(II) chloride (70 mg, 0.10 mmol) and copper iodide (19 mg, 0.10 mmol) were stirred in a Schlenk flask under vacuum for 30 min. 5-Iodo-3-*tert*-butylsalicylaldehyde (500 mg, 1.62 mmol), 1,3,-diethynylbenzene (113 mg, 0.90 mmol), NEt_3 (5 mL), and tetrahydrofuran (THF, 5 mL) were added, and the reaction mixture was stirred under argon at 45 °C for 18 h. The reaction mixture was poured into 10% aqueous NH_4Cl (20 mL) and extracted with CH_2Cl_2 (3 × 10 mL). The combined organic fractions were washed with water, dried over $MgSO_4$, and concentrated. The crude product was purified by flash chromatography on silica gel (CH_2Cl_2/pentane, 1:54:5) to yield the meta compound as yellow crystals (mp 173 °C, 133 mg, 31%): ^{1}H NMR ($CDCl_3$, 400 MHz) 1.37 (s, 18*H*), 7.28 (t, J = 8.0 Hz, 1*H*), 7.42 (dd, J = 7.6 Hz, J = 1.6 Hz, 2*H*), 7.55 (d, J = 2.0 Hz, 2*H*), 7.60 (d, J = 2.0 Hz, 2*H*), 9.81 (s, 2*H*), 11, 88 (s, 2*H*); ^{13}C NMR ($CDCl_3$, 100 MHz) 29.1, 35.0, 87.5, 89.0, 114.0, 120.5, 123.5, 128.6, 131.1, 134.4, 135.2, 137.1, 139.0,

161.4, 196.7. HRMS (ES) *m/e*: [M^+] calcd for $C_{32}H_{30}O_4Na$, 501.2042; found, 501.2029.

III. Results

A. Molecular Family. The class of molecules[48,49] studied are shown in Figure 1.[51] Members of this class of oligo-phenylene-ethynylenes) are interesting model molecules for the build up of one- and two-dimensional molecular nanostructures in a bottom-up approach and are in particular proposed as promising candidates for conducting organic wires in molecular electronics.[52,53] The molecules consist of a central benzene ring with two or three ethynylene spokes extending from it. For the two-spoke molecules, the para[49,50] and meta compounds, the angle between the spokes is 180° and 120°, respectively, and for the three-spoke compound,[48,49] the angle is 120°. Each ethynylene spoke is connected to a *tert*-butyl substituted salicylaldehyde moiety (a benzene ring with an aldehyde group, a hydroxyl group, and a *tert*-butyl group). The backbone of all three molecules consists of a conjugated π system. Previous studies have shown that such conjugated systems preferentially align parallel to metal surfaces[29] in order to maximize the van der Waals (vdW) interaction with the surface.

In the gas phase, the terminal salicylaldehyde moiety has freedom of rotation around the ethynylene spoke. (The energy barrier toward rotation for the para compound is determined to be 0.037 eV.)[41] When the molecules adsorb with the π system parallel to the surface, this rotation is hindered, leading to two possible orientations for each terminal moiety. The resulting surface conformers are summarized in Figure 2. Some of the conformers do not have a mirror plane perpendicular to the surface and are hence chiral.[29] To distinguish the different conformers, we note for each terminal group whether the *tert*-butyl group is to the left (L) or to the right (R) when looking along the spoke from the central benzene ring (and top-down on the molecule on the surface). For the meta compound, the order of the terminal groups is taken to be counterclockwise in the enclosed angle.

For the para compound, there are two salicylaldehyde moieties yielding 2^2 combinatorial possibilities, RL, LR, RR, and LL. RL and LR are identical, however, connected with a C_2 rotation around the surface normal. This leaves three distinct surface conformers as shown. The RR and LL conformers are enantiomers. Similarly, in the case of the meta compound, there exist four combinatorial possibilities, but because of the bent geometry of the molecule, the RL and LR species are no longer equivalent. Hence, we expect four different surface conformers with RR and LL being enantiomers. Finally, in the case of the three-spoke compound, there are three salicylaldehyde moieties, leading to 2^3 combinatorial possibilities, some of which are related by a C_3 rotation around the surface normal. As illustrated in Figure 2, we expect for the three-spoke compound to find four different conformers grouped as two pairs of enantiomers.

B. Molecular Imaging Modes. Following deposition at a coverage below saturation of the first monolayer, the three species are observed to self-assemble into large (several hundred ångströms wide) monomolecular high islands (see Figure 3a). The herringbone reconstruction of the Au(111) surface does not appear to be perturbed by the molecular adsorption, as the characteristic corrugation of the reconstruction clearly is observed to modulate the height of the adsorbed molecular overlayers, as shown in Figure 3b.

The individual molecules are revealed in high-resolution images acquired inside the islands as displayed in Figure 4. Two primary STM imaging modes are observed: In the majority of

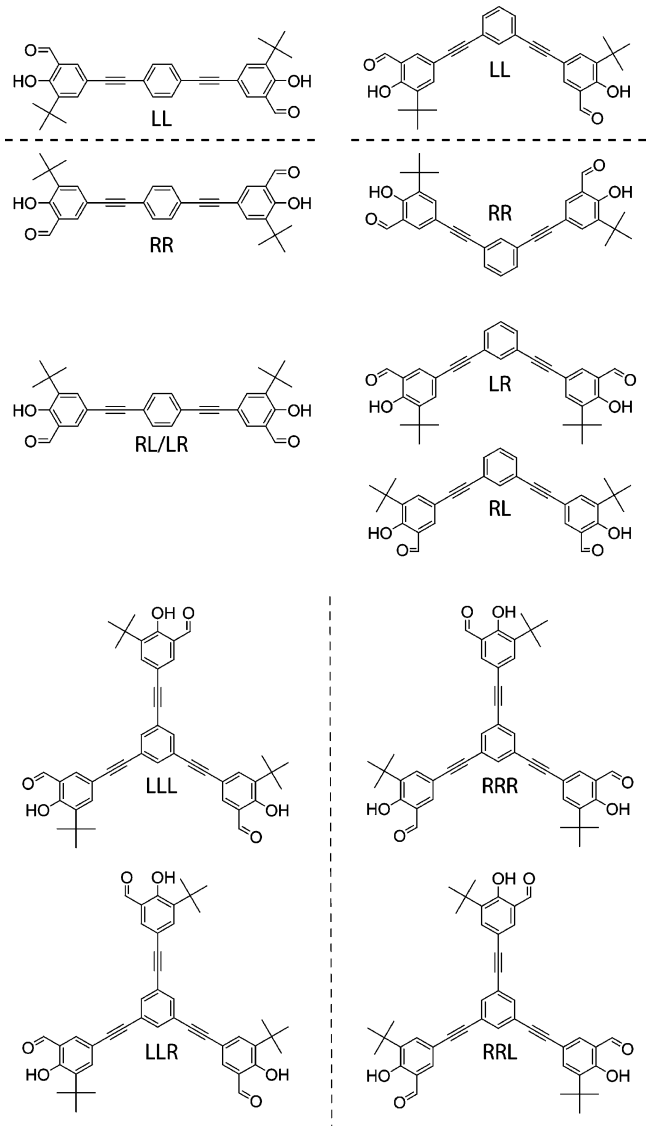

Figure 2. Surface conformers of the molecules (see text for naming scheme). Top left: the para compound has three conformers, two of which are enantiomers. Top right: the meta compound has four conformers, two of which are enantiomers. Bottom: the three-spoke compound has four conformers, grouped as two times two enantiomers. Dashed lines indicate mirror planes.

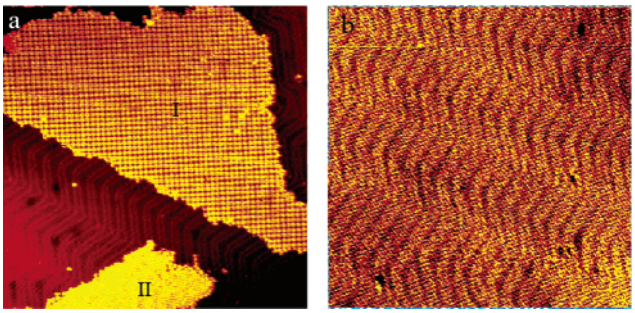

Figure 3. (a) Examples of coexisting monomolecular high islands formed from para molecules. I: grid structure. II: brick wall structure. (b) The Au(111) herringbone reconstruction is visible as a height modulation in the molecular islands (here formed by the meta molecules). Image sizes 1550 × 1550 Å^2.

the images, the topography is dominated by bright protrusions at the ends of the molecules (Figure 4b,e,h). These protrusions which are attributed to the *tert*-butyl groups in agreement with other studies[26,54,55] appear 2.40 ± 0.02 Å high compared with

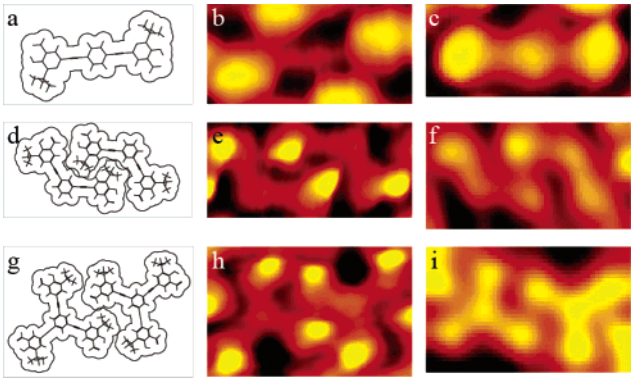

Figure 4. STM imaging for the three molecular species: left column: stick model of the molecules including their van der Waals radii.[46] The molecular orientation and conformation is chosen to approximate the accompanying STM images. Center column: STM imaging mode characterized by prominent *tert*-butyl groups (*tert*-butyl mode). Right column: imaging mode revealing the molecular backbone (π mode). Top row: para compound. Center row: meta compound. Bottom row: three-spoke compound.

the underlying surface and are positioned off-axis with respect to the ethynylene spokes, and thus they allow us to determine the molecular conformation.

An alternative imaging mode is observed where only the aromatic molecular backbone (π system) is visible, revealing the characteristic shape of the molecule (Figure 4c,f,i). We will refer to these two imaging modes as *tert*-butyl and π-system mode, respectively. Since we have not observed any correlation between specific tunneling parameters and appearance of the molecules, we attribute the two modes to different states of the STM tip, presumably caused by attachment and detachment of molecules at the tip apex.[13] As displayed in Figure 4, the π-system imaging mode clearly reveals that the molecules indeed adsorb with their backbone parallel to the surface.

C. Para Compound. The para compound[41] dominantly forms two coexisting adsorption phases, referred to in the following as the brick wall and grid structures, respectively (see also Figure 3a).

1. Brick Wall Structure. STM images of the brick wall adsorption structure are shown in Figure 5a,b. From the STM images obtained in the π-system imaging mode (Figure 5a), the molecules are observed to arrange themselves into a regular tiling pattern in which all molecular backbones are parallel to each other. The molecules are aligned end-to-end in rows with adjacent rows being shifted relative to each other by half the repeat distance along the rows as in the stacking of bricks in a wall. Figure 5c shows the structural model of the brick wall phase with the unit cell approximated as in Table 1.

The packing density for the brick wall structure $A_{vdW}/A_{mol} = 0.80$ (see Table 1) shows that in this phase the molecules are packed rather efficiently. The high-symmetry direction of the overlayer does not coincide with the high-symmetry direction of the substrate, and the molecular overlayer in combination with the substrate therefore exhibits adsorption-induced organizational chirality.

When observed in the *tert*-butyl imaging mode (Figure 5b), the brick wall structure appears less ordered because the molecules assume different surface conformations placing the *tert*-butyl group differently with respect to the molecular backbone. Consequently, the structure is not truly periodic.

The observed structure can be rationalized by considering the conformers and intermolecular interaction motifs displayed in Figure 5d,e. The tables in Figure 5 show probabilities, *P*,

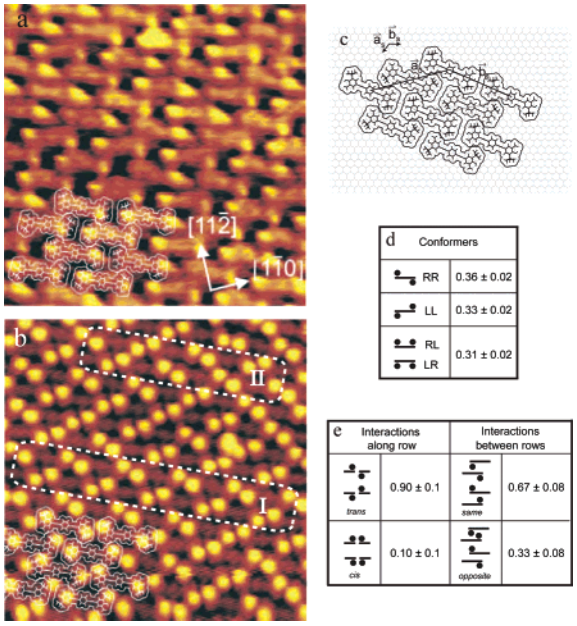

Figure 5. Brick wall structure formed by the para molecules. (a) STM image obtained in the π-system imaging mode (Size 120 × 120 Å^2). (b) STM image in the *tert*-butyl imaging mode (size 120 × 120 Å^2). I: defect free region. II: defect rich region, see text. The imposed structural models in the images are not fitted to the specific images but assign instead a defect free arrangement. Consequently, the end-group orientation in the models does not necessarily correspond to the orientation of the underlying molecules. (c) Tentative adsorption geometry. (d) Observed molecular conformers and (e) intermolecular arrangements. Lines and circles indicate molecular backbones and *tert*-butyl groups, respectively.

determined from analysis of STM images, of finding (i) the different surface conformers of the molecule, (ii) the different possible configurations for head-to-head intermolecular arrangements (*tert*-butyl groups on adjacent molecules either at the same side, cis, or opposite side, trans, of the line connecting two molecules), and (iii) the different possible configurations for side-to-side intermolecular arrangements (*tert*-butyl groups on adjacent molecules either pointing in the same or opposite directions). The positions of the *tert*-butyl groups on neighboring molecules or within the same molecule are clearly correlated. The dominant intermolecular ordering motif is to have the *tert*-butyl groups lying trans where molecules meet head-to-head ($P = 0.9 \pm 0.1$) and pointing to the same side where molecules meet side-to-side ($P = 0.67 \pm 0.08$). This ordering gives rise to a structure such as the one in the region marked I on Figure 5b, and this idealized structure is the one depicted in Figure 5c. To realize these two preferred intermolecular configurations, the intramolecular conformation must be either LL or RR, and alternating rows must consist of molecules entirely in the LL/RR conformation, respectively. This suggests that the preference for RR/LL intramolecular conformations ($P = 0.69 \pm 0.03$) as opposed to RL/LR ($P = 0.31 \pm 0.02$) results from the specific tiling pattern and intermolecular interactions rather than from intramolecular interactions between the two ends of a given molecule (which are spaced far apart compared with the distance to adjacent molecules). A significant proportion ($P = 0.33 \pm 0.08$) of the side-to-side interactions have the *tert*-butyl groups pointing in opposite directions, giving rise to structures as that in the region marked II on Figure 5b. The minority population of molecules in the RL/LR conformation results from this type of structure.

2. Grid Structure. The second phase exhibited by the para molecule is the grid structure shown in the STM images of

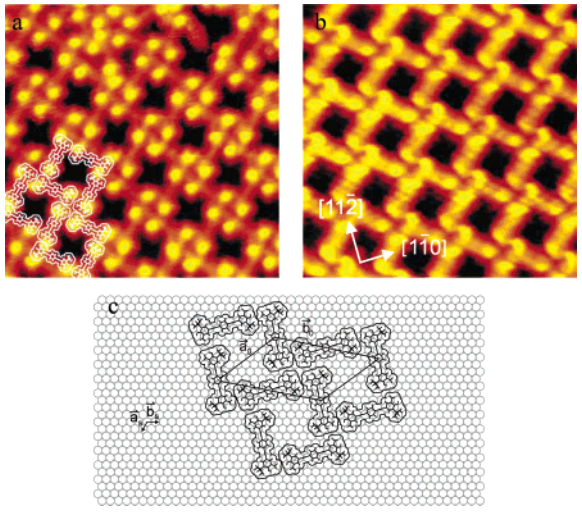

Figure 6. Nanogrid phase formed by the para compound. STM images in (a) the *tert*-butyl mode with superimposed structural model, and (b) π-system mode. Note that the domains shown in a and b are of opposite chirality as seen by the different sense of rotation for the central windmill motif. Image sizes 140 × 140 Å^2. (c) Tentative adsorption geometry.

Figure 6a,b, depicting the structure in the *tert*-butyl and π-system imaging modes, respectively. The primary structural motif is a windmill-like arrangement of four molecules joined in a common node. Each molecule connects two such adjacent nodes producing an extended, highly ordered network with openings bounded by four molecules. For the parameters of the unit cell, see Table 1. The grid structure is considerably more open than the brick wall phase discussed above ($A_{vdW}/A_{mol} = 0.58$). Since the molecules are not oriented along high-symmetry directions of the substrate, the molecular overlayer in combination with the substrate exhibits adsorption-induced organizational chirality.

The orientation of the *tert*-butyl groups is completely ordered in the grid phase. As seen from Figure 6a, the *tert*-butyl group always points away from the central node of the windmill motif. The grid phase is thus truly periodic, in contrast to the structure described above which only showed periodicity in the tiling of the molecular backbones. The tiling pattern in the grid phase is chiral since the central windmill motif can be constructed with two opposing rotational directions. (The two domains shown in Figure 6a,b have an opposite sense of rotation for the windmill motif, as is appreciated by comparing the superimposed structural model in a with the backbone image in b.) The chirality of the surface conformers participating in the structure is completely correlated with the chirality of the backbone tiling: In order for the *tert*-butyl groups to point away from the central node, only LL conformers are found in the chiral domain shown in Figure 6a and only RR conformers participate in the domain of opposite chirality shown in Figure 6a. The structure thus shows perfect ordering of the RR/LL enantiomers into enantiopure domains, and the non-chiral RL/LR conformers do not participate.

D. Meta Compound. The meta compound exhibits only one distinct adsorption phase, displayed in the STM image of Figure 7a (in which both molecular backbones and *tert*-butyl groups are readily recognized); see Table 1 for details. The dominant packing motif is a pair of molecules, rotated by 180° with respect to each other and oriented with an ethynylene spoke of each pointing toward the vertex formed from the two spokes of the other. These pairs stack into rows running along the ⟨112⟩ direction. The molecular pair motif is chiral and can be realized in two enantiomeric forms as shown in Figure 7c. All pairs

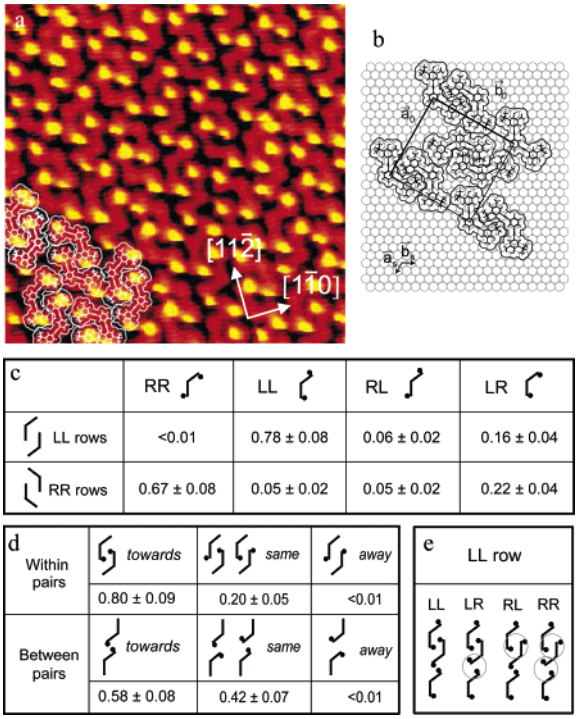

Figure 7. Adsorption structure formed by the meta molecule. (a) STM image (120 × 120 Å^2). (b) Tentative adsorption geometry. (c) Distribution of different surface conformers in rows dominated by LL and RR conformers, respectively. (d) Distribution of relative orientations of *tert*-butyl groups on neighboring molecules. Top row: within the nested pairs. Bottom row: between the nested pairs along the molecular rows (the numbers are derived from analysis of both chiralities of the tiling motif). (e) Illustration of the consequence of introducing other surface conformers (center-most molecule) into rows consisting of LL molecules. The circles indicate interactions that are unfavorable due to steric hindrance, loss of vdW interaction, or both.

within a given row are of the same chirality, and the rows alternate between the two possible enantiomeric forms. The unit cell is rectangular and contains two glide line symmetry elements connecting the molecular pair placed in the unit cell with the pairs of opposite chirality placed at the corners of the cell. The overall tiling pattern is thus *not* chiral despite being formed from chiral subunits. The packing density is $A_{vdW}/A_{mol} = 0.85$.

The probabilities for finding different conformers and intermolecular configurations has been investigated. The analysis with respect to surface conformers has been done separately for the two types of rows with opposite chirality in the pair motif (see Figure 7c). The predominant conformers are the chiral LL/RR species which are observed with a probability of $P = 0.7 \pm 0.1$. The two types of rows are each strongly dominated by one of the two chiral conformers: The probability of finding an RR/LL conformer in a row dominated by LL/RR conformers is only a few percent. Of the two nonchiral conformers (RL and LR), the LR conformer is dominant in both types of rows. Probabilities, P, for different intermolecular configurations, reflecting possible nearest neighbor intermolecular interactions, are summarized in Figure 7d. Both within the molecular pairs and between them (along the direction of the molecular rows), there is a preference for having *tert*-butyl groups on neighboring molecules oriented toward each other ($P = 0.80 \pm 0.09$ within pairs and $P = 0.58 \pm 0.08$ between pairs). These predominant orientations of the *tert*-butyl groups favor RR/LL species depending upon the chirality of the tiling motif, as illustrated in Figure 7e. When a deviating conformer is inserted into a row formed from LL conformers, nonpreferential interaction configurations result in either one (LR or RL) or both (RR)

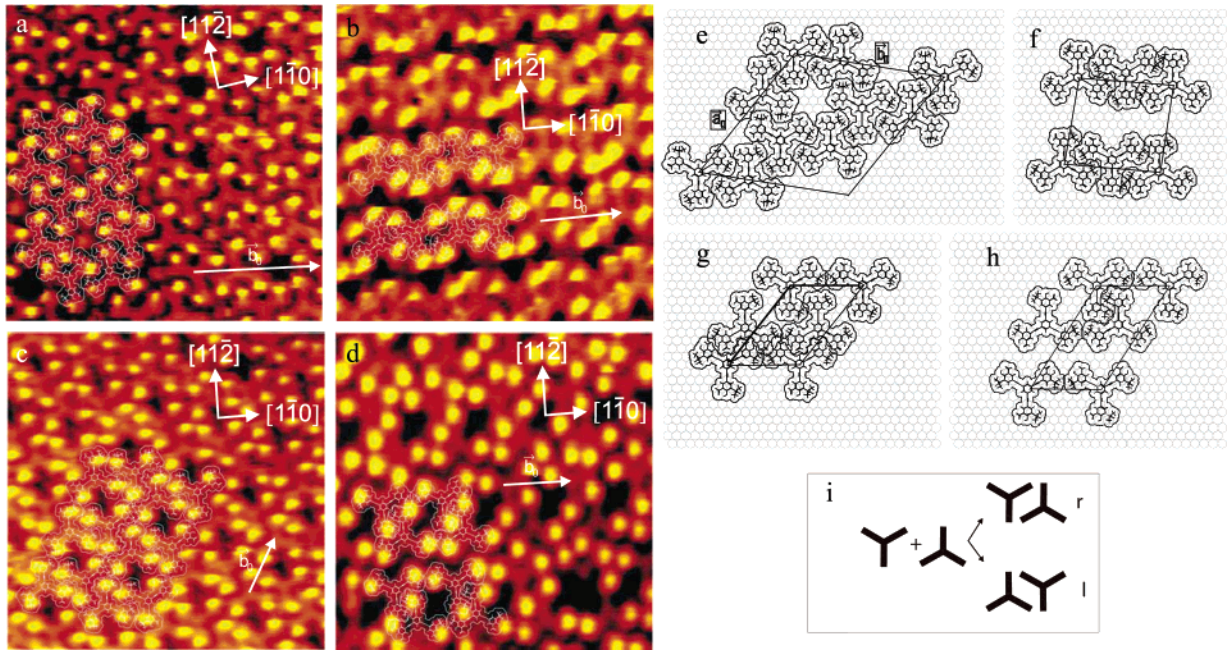

Figure 8. Adsorption structures formed by the three-spoke molecule. STM images and tentative adsorption geometries of the (a + e) hexagonal structure, (b + f) row structure, (c + g) dense ladder structure, and (d + g) open ladder structure. Image sizes 120 × 120 Å^2. (i) Chiral interaction motif observed for all four packing patterns. One molecule of the unit cell can be either positioned to the right (r) or to the left (l) of the spokes of the other molecule, as seen from the central benzene ring.

neighbors, explaining the ordering of probabilities for finding the different conformers in LL rows.

E. Three-Spoke. The three-spoke compound is found to aggregate into four different adsorption structures as shown in the STM images of Figure 8a−d. We will refer to these structures as hexagonal (a), row (b), dense ladder (c), and open ladder (d), respectively (see also Table 1). We could not attribute the formation of one specific phase to a special preparation or imaging condition, rather, the structures seem to coexist for a wide range of parameters.

The three-spoke compound adsorbs with its spokes along high-symmetry [11$\bar{2}$] directions. This can be realized in two distinct ways, related by a 60° rotation of the molecule. We will refer to these orientations as "up" and "down", respectively. Two molecules of up and down orientation close-pack with an end-group of one molecule lying in the vertex formed by two arms of the other (compare Figure 8i). This arrangement is chiral and can be formed in two distinct ways, termed "r" (right) and "l" (left). This motif is somewhat similar to the one adopted by the meta compound.

In the hexagonal structure, the molecules are arranged into six-membered rings, each molecule belonging to three such interlocked rings. As one proceeds along the ring perimeter, the molecules alternate between up and down. All spokes of the molecules participate in the described chiral interaction motif. In the domain shown in Figure 8a, all of these motifs are of r chirality. The molecular organization is thus chiral in itself. In the corresponding mirror domain (not shown), all interaction motifs are of the l type. The unit cell and a possible adsorption geometry for the molecules on the Au(111) plane are shown in Figure 8e.

In the row structure, Figure 8b, the molecules are arranged into rows oriented slightly off the [1$\bar{1}$0] direction, therefore the structure has organizational chirality. Proceeding along a row, the molecules alternate between up and down. Two spokes on each molecule participate in the chiral interaction motif while the last points toward the edge of the row. The interaction motifs alternate between the r and l chirality.

TABLE 2: Distribution of the Possible Conformations in the Four Structures Formed by the Three-Spoke Molecule[a]

conformer	hexagonal	row
LLL	0.01 ± 0.01	0.05 ± 0.02
LLR	0.15 ± 0.05	0.46 ± 0.06
LRR	0.42 ± 0.08	0.49 ± 0.06
RRR	0.42 ± 0.08	0.02 ± 0.02

[a] Note that, for structures with local organizational chirality, the distribution is for one of the possible domains; in mirror domains the inverse distribution is found.

The dense and open ladder structures (Figure 8c,d) are closely related. In both structures, pairs of molecules, arranged in the chiral interaction motif, stack along the ⟨110⟩ direction by joining sideways (best appreciated in Figure 8d). The resulting "ladder-like" structures are spaced somewhat apart in the open ladder structure while they are closely packed in the dense ladder structure. The chiral interaction motif is assumed for one/two spoke(s) per molecule in the open/dense ladder structures, respectively. The interaction motifs are exclusively of one chirality (l for both domains shown in Figure 8c,d), and the structures are thus chiral. Suggested adsorption geometries for the two structures are shown in Figure 8g,h while unit cells and packing densities are listed in Table 1.

Also for this compound, the orientation of the salicylaldehyde moieties presents an additional level of organization compared with the molecular tiling patterns. The probabilities of finding the different molecular surface conformers in the hexagonal and row structures, respectively, have been evaluated from the STM images and are displayed in Table 2 (the numbers are for domains with the same chirality of the tiling pattern as those shown in the STM images of Figure 8). The distribution for the hexagonal structure is highly asymmetric, favoring the R orientation, while the distribution for the row structure is symmetric within the error bars, with the RRR/LLL conformers occurring with a somewhat lower probability than expected for a random distribution. The preference for different surface conformers is thus strongly affected by the particular tiling

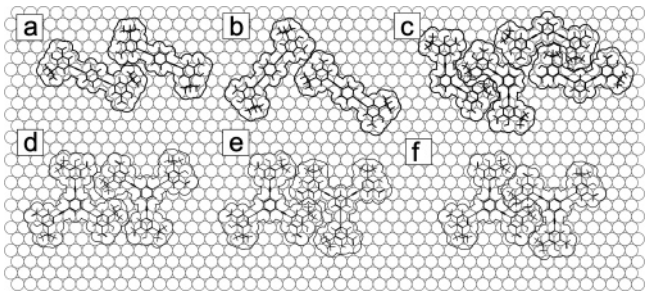

Figure 9. Models of the adsorption structures giving details on the adsorption site and orientation (a) brick wall phase and (b) grid-phase of the para compound, (c) meta compound, (d) hexagonal and row, (e) dense ladder, and (f) open ladder phase of the three-spoke compound. In contrast to some of the models earlier, here, all structures formed by the meta and the three-spoke compound are shown in the l tiling pattern.

pattern assumed by the molecules. Both the hexagonal and row structures are dominated by the chiral packing motif with terminal groups positioned in the vertex of a neighboring molecule. In this arrangement, the end group can be oriented with its *tert*-butyl group pointing either toward or away from the vertex. From an analysis of the STM images, we find the *tert*-butyl group to predominantly point toward the neighboring vertex, which occurs with probabilities of 0.75 ± 0.07 and 0.72 ± 0.05 for the hexagonal and row structures, respectively. In the hexagonal structure, where only intermolecular packing of the r type occurs (in the analyzed domain), this requires the molecules to predominantly assume the R rotational orientation of the end group. In the row structure, on the other hand, the two end groups per molecule that participate in the chiral packing motif are in vertices of r and l orientation, respectively, while the third end group resides in a fairly symmetric environment. As a result, the assumed molecular conformers become symmetric with respect to the R/L orientation, and RRR/LLL conformers become less likely.

The correlation between tiling pattern and adopted molecular conformations is more complicated for the two ladder structures and has not been analyzed in detail.

IV. Discussion

A. Adsorption Geometries. In this section, the adsorption geometries for the three molecular compounds will be compared. The orientation of the molecules with respect to the substrate lattice can be determined from STM images obtained in the π-system imaging mode, where the molecular backbone is revealed. However, a more precise determination can be obtained from analysis of the bright protrusions characterizing the *tert*-butyl groups. The position of these protrusions with respect to the molecular backbone was determined from analysis of three-spoke molecules with different conformations but in equivalent lattice sites (compare Figure 9). The analysis reveals that a line connecting the center of the molecule with the bright protrusion lies at an angle of 9° with respect to the molecular backbone which allows us to determine the orientation of the backbone from images taken in the *tert*-butyl imaging mode. The corresponding angle for a line connecting the center of the molecule with the central C of the *tert*-butyl group is 18°, showing that the center of the bright protrusion observed in the STM images lies somewhat off the geometric center of the *tert*-butyl group.

The registry of the molecules with respect to the substrate could not be determined, since we were not able to obtain atomic resolution of the Au(111) substrate simultaneously with imaging the molecules. In the models shown in Figure 9, we therefore assume that each of the compounds adsorb with its spokes in equivalent geometries. The molecules with 120° between the spokes (meta and three-spoke) are thus assumed to adsorb with its center at a surface site with C_3 symmetry (threefold hollow site and on-top site) whereas the molecules with 180° between the spokes (para) are assumed to find sites with C_2 symmetry (bridge site and on-top site).

For the brick wall phase of the para compound, the molecular backbone forms an angle of $\delta = 23°$ with the $\langle 110 \rangle$ direction. The requirement of placing both molecules in the unit cell with their centers at C_2 sites can be fulfilled by placing the first molecule in an on-top site and the second molecule $(1/2)\vec{a}_o$ away from it in a bridge site. The resulting adsorption geometry is shown in Figure 9a.

In the grid phase, the two molecules in the unit cell are not equivalent, since one has $\delta = -11°$ and the other has $\delta = 25°$. The enclosed angle of the rhombic holes in the structure is thus 96° (11° + 60° + 25°). Both molecules can be placed at an on-top site if the vector between them is $(1/2)\vec{b}_o$. This unit cell is depicted in Figure 6c. Given the uncertainty (~5%) in our measurements, it is possible that the molecules with $\delta = 25°$ in the grid phase have an identical adsorption geometry to the molecules in the brick wall phase, where $\delta = 23°$ was determined.

The meta and the three-spoke compounds are both found to be oriented with their spokes along $\langle 112 \rangle$ directions, that is, perpendicular to a close-packed direction of the substrate. Placing the meta and three-spoke compound with their centers on C_3 sites gives the adsorption geometries depicted in Figure 9c−f. Despite the similarity of the molecules, the intermolecular separations are not always identical; the meta compound shows the same local geometry inside the pairs as the open ladder structure, and the hexagonal phase is similar to the row phase.

B. Interactions. The aldehyde and hydroxyl groups were originally introduced on the compounds used in this study in order to enable formation of intermolecular hydrogen bonds. However, in most of the observed adsorption structures, the molecules assume orientations on the substrate that place these groups too far from each other to be consistent with formation of O−H−O hydrogen bonds. For most of the structures, we instead observe that the geometric arrangement and intermolecular distances fit a van der Waals close-packing. The observed structures which do not favor intermolecular hydrogen bond formation may be caused by the molecules having an intramolecular hydrogen bond ($E_b = 0.34$ eV/group[56]) between the aldehyde and hydroxyl groups which has to be broken before intermolecular hydrogen bonds can form. Consequently, only intermolecular hydrogen bonds that are strong enough to compensate for the breaking of this intramolecular bond will be energetically favorable.

A special case is the grid phase formed by the para compound. Compared with the brick wall phase, the grid phase has a lower packing density and shows a higher degree of conformational order for the participating molecules. This points toward the existence of a directional intermolecular interaction compensating for the loss of vdW−intermolecular interaction resulting from the reduced packing density. We speculate that the molecular arrangement in the nodes of the grid structure facilitates the formation of an intermolecular hydrogen-bonding network connecting hydroxyl and aldehyde groups on neighboring molecules. This possibility has been investigated by

modifications of the functional groups of the para compound. Results from this investigation will be presented elsewhere. Similar open grid like structures have not been observed for the meta and the three-spoke compounds. For the three-spoke molecule with C_3 symmetry, a bonding pattern with four interacting head groups would cause overlap between molecules from adjacent nodes. A pattern based on three interacting groups is in principle possible, but the reduced number of potential hydrogen bonds may make such a structure energetically unfavorable. For the meta compound, a homochiral structure based on the fourfold node is conceivable, but the lack of C_2 symmetry of the meta molecule implies that an arbitrary surface conformer cannot adjust itself to an existing network solely by an end group flipping process[41] (see next section).

Aside from the conformationally ordered grid phase, we also found a certain but less pronounced order of the head groups in the other structures. This ordering must result from interactions between the end groups and the surrounding molecules. Each end group can be oriented in two ways with respect to the surroundings, as the *tert*-butyl group is positioned either to the right (R) or to the left (L) when observed along the spoke from the central benzene ring (see Figure 2). This leads therefore in many cases to favored and unfavored end group orientations. By assuming a Boltzmann distribution ($(N_{uf}/N_f) = \exp(-(\Delta E/k_B T))$) the energy difference, ΔE, between the favored and the unfavored end group arrangement can be estimated by the number, N_f (N_{uf}) of end groups having a favored (unfavored) orientation. As outlined, the para compound in the brick wall phase has a dominant ordering motif in which *tert*-butyl groups are lying trans where molecules meet head-to-head and point to the same side where molecules meet side-to-side. Statistical analysis of several hundred molecules gives 93% trans head-to-head arrangements at 197 K and 58% end groups with same side-to-side arrangements at 191 K corresponding to an energy difference between cis/trans pairs of 0.04 eV[41] and same/opposite arrangements of ~0.005 eV. Similarly in the structure formed by the meta compound and the row and hexagonal structure of the three-spoke compound, the molecular spokes oriented toward a vertex of a neighboring molecule preferentially have the *tert*-butyl group oriented toward the vertex. The energy gain associated with this arrangement, compared with having the end group oriented oppositely, is estimated to be between 0.014 and 0.020 eV. The other observed interaction motifs yield similar energies. Consequently, the potential energy landscape controlling the conformational order of the molecules in these structures has only small variations in the range of 0.005−0.05 eV. The interaction between the end groups in the grid structure may be larger, as no defects are found in the interior of that structure.

C. Molecular Dynamics and Chiral Ordering. The para, meta, and three-spoke compounds all form structures where there is a clear correlation between the chirality of the molecular tiling patterns and the conformation of the embedded surface conformers. In this section, we investigate in further details the processes responsible for the creation of order. The formation and ordering of the molecular structures is a dynamical process in which the structures interchange molecules with the lattice gas and in which molecules embedded in the structures switch their conformation in order to accommodate to the tiling pattern of the network. These dynamical phenomena can be revealed by superimposing two time-separated STM images of the same portion of the surface such that the first image colored blue and the second image colored orange results in stationary features appearing gray, whereas the initial (final) position of a moving feature appears blue (orange).

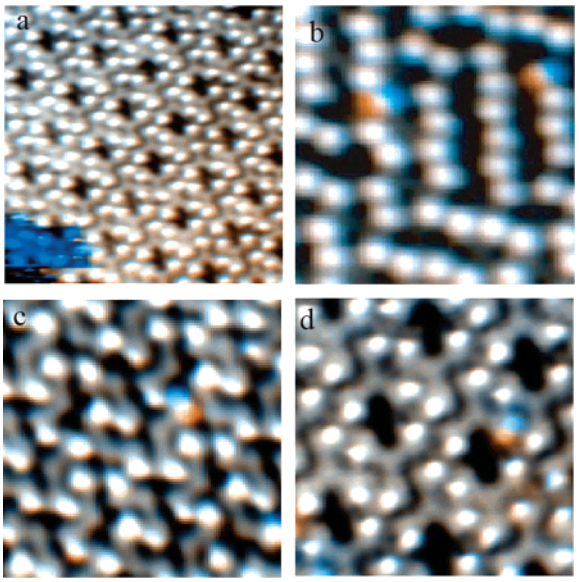

Figure 10. Dynamics of the molecules shown by overlay images where the initial/final image is color coded blue/orange. (a) STM images (150×150Å^2) revealing three-spoke molecules leaving the island. (b−d) STM images (70×70Å^2) revealing conformational changes inside the islands for the para compound (b), meta compound (c), and the three-spoke compound (d).

This color coding is used in Figure 10a, where the three-spoke molecules originally embedded in an island (blue) are seen to detach and diffuse into the lattice gas (orange).[57] The networks thus interchange molecules with the lattice gas at the imaging temperatures of 140−170 K. As single molecules are never observed outside the condensed phases, the molecules in the two-dimensional gas phase are thus highly mobile.

By overlaying images as the ones shown in Figure 10b−d, we observe that the bright protrusions attributed to the *tert*-butyl groups occasionally shift position from one side of a molecular spoke to the other side. We interpret this to be arising from a rotation of the end group around one molecular spoke such that the *tert*-butyl group is transferred from one side of the molecular backbone to the other side. The blue (orange) protrusion reveals the initial (final) position of a moving *tert*-butyl group. This phenomenon was described previously for the para compound,[41] but is shown here to be a general phenomenon for this class of compounds. The spontaneous switching implies that the molecules are not completely fixed by the substrate but can change between the different surface conformers after adsorption. For the brick wall structure formed by the para compound, all of the structures formed by the three-spoke compound, and the structure formed by the meta compound, switching is observed in the interior of the domains. However, for the grid phase formed by the para compound, we only observe switching at the edge of the islands, reflecting the stronger intermolecular interaction in this structure.

The rates of conformational switching are controlled by the potential energy landscape experienced by the molecule, and rates from an unfavored to a favored end group configuration are thus higher than rates from a favored to an unfavored configuration.

The rates $\Gamma_{trans-cis}$ and $\Gamma_{cis-trans}$ between the trans and cis configurations of the head groups found in the brick wall structure for the para compound have been determined[41] in detail from the analysis of STM videos acquired at a range of sample

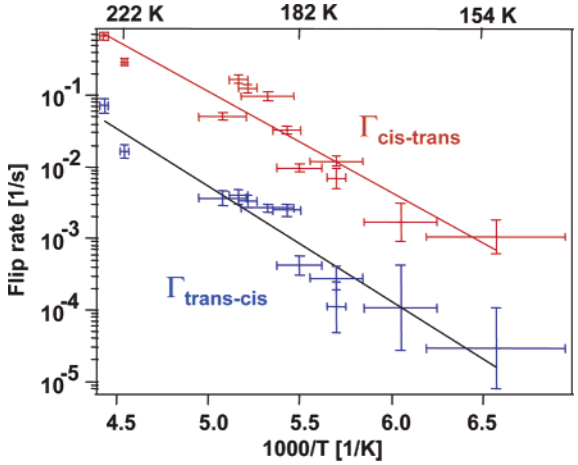

Figure 11. Arrhenius plot[41] of the rate for cis−trans and trans−cis flips in the brick wall structure. Horizontal error bars indicate the temperature interval over which the STM data used to evaluate the respective data points were acquired. Vertical error bars represent one standard deviation.

temperatures between 140 and 230 K. The details of the analysis are described under Methods. It fully takes into account the possibility of multiple flips between consecutive images. The determined rates are plotted in Figure 11, and the cis−trans rates are indeed higher than their counterparts. Some of the scatter in the data results from the less strong side-to-side interactions between molecules in adjacent rows which depend on the local area imaged in a given STM movie. From fit to the Arrhenius form, $\Gamma = \nu \exp(-E/k_BT)$, where ν is the prefactor, E is the activation energy, k_B is the Boltzmann constant, and T is the temperature, we find $E_{trans-cis} = 0.32 \pm 0.03$ eV and $E_{cis-trans} = 0.28 \pm 0.03$ eV, consistent with the determined energy difference between cis and trans pairs of 0.04 eV. The pre-factors $\nu_{trans-cis} = 10^{5.8\pm0.8}$ s^{-1} and $\nu_{cis-trans} = 10^{6.1\pm0.8}$ s^{-1} are considerably smaller than the standard $k_BT/h \sim 10^{12}$ s^{-1} found for other activated processes on surfaces, such as diffusion.[14,15,18] The energy barrier for meta and three-spoke molecules is likely to be similar to the barrier of ~0.3 eV found for the para molecule as all these compounds have been observed to switch conformation in the same temperature window.

The origin of the energy barrier has been investigated by theoretical modeling based on density functional theory calculations as described previously.[41] In the model, the energy difference between the start configuration and the transition state is comprised of a decrease in molecule−substrate interaction with a cost of 0.2 eV and a bending of the molecular axis by 25° in the transition state with a contribution of 0.17 eV. The total energy barrier for the conformational change is therefore estimated to 0.37 eV, comparable to the experimental value. The bulky *tert*-butyl group was found to induce a 18° tilting of the benzene ring in the optimum adsorption configuration.

The above-described switching mechanism enables an accommodation pathway toward chiral segregation into homochiral domains, in which molecules adjust their conformation to the surrounding tiling pattern.[41,42] This accommodation mechanism was revealed most clearly for the para compound in the grid phase where we found the pronounced correlation between the chirality of the tiling pattern (clockwise or counterclockwise rotation of the windmill motif) and the chirality of the condensed molecules (RR/LL). Because of the strong binding in the nodes of the network, the molecules in the grid structure were only observed to switch conformation at the island edges[41] at the imaging temperature. Consequently, here, we observed the growth of defect-free homochiral domains directly from heterochiral molecules.

For the other structures observed, where the chiral ordering is less pronounced, the correlation between the tiling pattern of the structures and the conformation of the embedded molecules also results from switching occurring after growth of the structures. Ultimately, this results in an equilibrium distribution of surface conformers which is determined by the potential energy landscape of the specific domain (such as the asymmetry in the LLL/RRR and LLR/RRL distribution found for the hexagonal phase of the three-spoke compound which is caused by one spoke orientation being energetically favored). To investigate whether growth occurs prior to conformational ordering, the three-spoke molecule was deposited onto a sample held at a low temperature of 95 K. The sample was subsequently slowly heated up during scanning in the STM. We observed that islands started growing at sample temperatures between 160 and 165 K. In this temperature window, the rate for the conformational switching is such that steady state can be reached within a few minutes. The two processes of aggregation and switching therefore happen simultaneously in these experiments.

The observed process of conformational switching may be general to a whole class of molecules that possess a rotational degree of freedom around a single bond which allows them to change their conformation even after adsorption. In addition to the molecules described in these studies, a candidate for such a process is, for example, 4-[*trans*-2-(pyrid-4-ylvinyl)]benzoic acid (PVBA).[36,58]

V. Conclusion

In conclusion, the three studied molecules tend to arrange themselves into van der Waals close-packed structures mainly determined by the shape of the molecule. In the structures, chiral ordering is observed both in the tiling pattern of the molecules and in the distribution of conformers. We find that the conformation of the embedded molecules is correlated with the arrangement of the tiling pattern, and we find that the interactions directing this ordering are fairly weak, in the order of 0.005−0.05 eV. For one compound, we observe a more open grid structure with complete conformational order, which we speculate may be due to more directional hydrogen bonding interactions between the functional groups.[59]

We observe that molecules at the island edges attach and detach. We therefore assume that the structures are in equilibrium with the lattice gas[57] and consequently even so with the other coexisting structures observed for the same compound. We find that all of the studied molecules can switch their conformation after adsorption by a rotation around the molecular spokes and that the observed conformational ordering inside the domains is enhanced by dynamical changes in the molecular conformation upon incorporation of the molecules into the islands. We observe how molecules accommodate to the structures and change their conformation after or during attachment to reach the state of highest binding energy. This accommodation procedure is effective as it reduces the mass transport compared with segregation procedures in which molecules reaching the islands only incorporate if they have the right conformation. In future studies,[41,42] the formation of global homochiral domains may be realized by seeding[35,40] the surface with a chiral template compound or by adsorbing the molecules on a chiral template surface.[34] The potential ability to form such homochiral surface layers is of high interest to

the field of heterogeneous asymmetric catalysis and even with respect to the understanding of the chiral asymmetry observed in nature.

Acknowledgment. We acknowledge support from the EU programs FUN-SMART and AMMIST, the Carlsberg foundation, the Danish Natural Science Research Council through funding for the iNANO center, the Danish Natural Research Foundation, and Aarhus University Research Foundation.

References and Notes

(1) Barth, J. V.; Costantini, G.; Kern, K. *Nature* **2005**, *437*, 671−679.
(2) Whitesides, G. M.; Gryzbowski, B. *Science* **2002**, *295*, 2418−2421.
(3) Furukawa, M.; Tanaka, H.; Sugiura, K.; Sakata, Y.; Kawai, T. *Surf. Sci.* **2000**, *445*, L58.
(4) Theobald, J. A.; Oxtoby, N. S.; Phillips, M. A.; Champness, N. R.; Beton, P. H. *Nature* **2003**, *424*, 1029−1031.
(5) Barth, J. V.; Weckesser, J.; Lin, N.; Dmitriev, A.; Kern, K. *Appl. Phys. A* **2003**, *76*, 645−652.
(6) De Feyter, S.; De Schryver, F. C. *Chem. Soc. Rev.* **2003**, *32*, 139−150.
(7) Pawin, G.; Wong, K. L.; Kwon, K.-Y.; Bartels, L. *Science* **2006**, *313*, 961−962.
(8) Schöck, M.; Otero, R.; Stojkovic, S.; Hümmelink, F.; Gourdon, A.; Lægsgaard, E.; Stensgaard, I.; Joachim, C.; Besenbacher, F. *J. Phys. Chem. B* **2006**, *110*, 12835−12838.
(9) Yokoyama, T.; Yokoyama, S.; Kamikado, T.; Okuno, Y.; Mashiko, S. *Nature* **2001**, *413*, 619−621.
(10) de Wild, M.; Berner, S.; Suzuki, H.; Yanagi, H.; Schlettwein, D.; Ivan, S.; Baratoff, A.; Güntherodt, H. J.; Jung, T. A. *Chem. Phys. Chem.* **2002**, *3*, 881−885.
(11) Berner, S.; de Wild, M.; Ramoino, L.; Ivan, S.; Baratoff, A.; Guntherodt, H. J.; Suzuki, H.; Schlettwein, D.; Jung, T. A. *Phys. Rev. B* **2003**, *68*, 115410.
(12) Lin, N.; Dmitriev, A.; Weckesser, J.; Barth, J. V.; Kern, K. *Angew. Chem., Int. Ed.* **2002**, *41*, 4779−4783.
(13) Gross, L.; Moresco, F.; Ruffieux, P.; Gourdon, A.; Joachim, C.; Rieder, K.-H. *Phys. Rev. B* **2005**, *71*, 165428.
(14) Linderoth, T. R.; Horch, S.; Lægsgaard, E.; Stensgaard, I.; Besenbacher, F. *Phys. Rev. Lett.* **1997**, *78*, 4978.
(15) Schunack, M.; Linderoth, T. R.; Rosei, F.; Lægsgaard, E.; Stensgaard, I.; Besenbacher, F. *Phys. Rev. Lett.* **2002**, *88*, 156102.
(16) Otero, R.; Hümmelink, F.; Sato, F.; Legoas, S. B.; Thostrup, P.; Lægsgaard, E.; Stensgaard, I.; Galvão, D. S.; Besenbacher, F. *Nature Mater.* **2004**, *3*, 779−782.
(17) Miwa, J. A.; Weigelt, S.; Gersen, H.; Besenbacher, F.; Rosei, F.; Linderoth, T. R. *J. Am. Chem. Soc.* **2006**, *128*, 3164−3165.
(18) Lauhon, L. J.; Ho, W. *J. Chem. Phys.* **1999**, *111*, 5633−5636.
(19) Chiaravalloti, F.; Gross, L.; Rieder, K.-H.; Stojkovic, S. M.; Gourdon, A.; Joachim, C.; Moresco, F. *Nature Mater.* **2007**, *6*, 30−33.
(20) Gimzewski, J. K.; Joachim, C.; Schlittler, R. R.; Langlais, V.; Tang, H.; Johannsen, I. *Science* **1998**, *281*, 531−533.
(21) Yanagi, H.; Mukai, H.; Ikuta, K.; Shibutani, T.; Kamikado, T.; Yokoyama, S.; Mashiko, S. *Nano Lett.* **2002**, *2*, 601−604.
(22) Jung, T. A.; Schlitter, R. R.; Gimzewski, J. K. *Nature* **1997**, *386*, 696−698.
(23) Moresco, F.; Meyer, G.; Rieder, K.-H.; Tang, H.; Gourdon, A.; Joachim, Ch. *Phys. Rev. Lett.* **2001**, *86*, 672−675.
(24) Loppacher, Ch.; Guggisberg, M.; Pfeiffer, O.; Meyer, E.; Bammerlin, M.; Lüthi, R.; Schlittler, R.; Gimzewski, J. K.; Tang, H.; Joachim, C. *Phys. Rev. Lett.* **2003**, *90*, 066107.
(25) Qiu, X. H.; Nazin, G. V.; Ho, W. *Phys. Rev. Lett.* **2004**, *93*, 196806.
(26) Schunack, M.; Rosei, F.; Naitoh, Y.; Jiang, P.; Gourdon, A.; Lægsgaard, E.; Stensgaard, I.; Joachim, C.; Besenbacher, F. *J. Chem. Phys.* **2002**, *117*, 6259−6265.
(27) Bonifazi, D.; Spillmann, H.; Kiebele, A.; de Wild, M.; Seiler, P.; Cheng, F. Y.; Güntherodt, H. J.; Jung, T.; Diederich, F. *Angew. Chem., Int. Ed.* **2004**, *43*, 4759−4763.
(28) Ernst, K.-H. *Top. Curr. Chem.* **2006**, *265*, 209−252.
(29) Barlow, S. M.; Raval, R. *Surf. Sci. Rep.* **2003**, *50*, 201−341.
(30) Ortega Lorenzo, M.; Baddeley, C. J.; Muryn, C.; Raval, R. *Nature* **2000**, *404*, 376−379.
(31) Kühnle, A.; Linderoth, T. R.; Hammer, B.; Besenbacher, F. *Nature* **2002**, *415*, 891−893.
(32) Lopinski, G. P.; Moffatt, D. J.; Wayner, D. D. M.; Wolkow, R. A. *Nature* **1998**, *392*, 909−911.
(33) Fang, H.; Giancarlo, L. C.; Flynn, G. W. *J. Phys. Chem. B* **1998**, *102*, 7311−7315.
(34) McFadden, C. F.; Cremer, P. S.; Gellman, A. J. *Langmuir* **1996**, *12*, 2483−2487.
(35) Parschau, M.; Romer, S.; Ernst, K.-H. *J. Am. Chem. Soc.* **2004**, *126*, 15398−15399.
(36) Weckesser, J.; De Vita, A.; Barth, J. V.; Cai, C.; Kern, K. *Phys. Rev. Lett.* **2001**, *87*, 096101.
(37) Chen, Q.; Richardson, N. V.; *Nature Mater.* **2003**, *2*, 324−328.
(38) Böhringer, M.; Schneider, W.-D.; Berndt, R. *Angew. Chem., Int. Ed.* **2000**, *39*, 792−795.
(39) France, C.; Parkinson, B. *J. Am Chem. Soc.* **2003**, *125*, 12712−12713.
(40) Fasel, R.; Parschau, M.; Ernst, K.-H. *Nature* **2006**, *439*, 449−452.
(41) Weigelt, S.; Busse, C.; Petersen, L.; Rauls, E.; Hammer, B.; Gothelf, K. V.; Besenbacher, F.; Linderoth, T. R. *Nature Mater.* **2006**, *5*, 112−117.
(42) Richardson, N. *Nature Mater.* **2006**, *5*, 91−92.
(43) Lægsgaard, E.; Besenbacher, F.; Mortensen, K.; Stensgaard, I. *J. Microsc.* **1988**, *152*, 663−669.
(44) See also www.specs.de.
(45) Barth, J. V.; Brune, H.; Ertl, G.; Behm, R. J. *Phys. Rev. B* **1990**, *42*, 9307−9318.
(46) *Titan*; Wavefunction, Inc. and Schrödinger, Inc., 1999.
(47) Neenan, T. X.; Whitesides, G. M. *J. Org. Chem.* **1988**, *53*, 2489−2496.
(48) Gothelf, K. V.; Brown, R. S.; Thomsen, A.; Nielsen, M. World Patent 2004050231, 2004.
(49) Nielsen, M.; Thomsen, A. H.; Jensen, T. R.; Jakobsen, H. J.; Skibsted, J.; Gothelf, K. V. *Eur. J. Org. Chem.* **2005**, *2005*, 342−347.
(50) Weigelt, S.; Busse, C.; Bombis, Ch.; Knudsen, M. M.; Gothelf, K. V.; Strunskus, T.; Wöll, Ch.; Dahlbom, M.; Hammer, B.; Lægsgaard, E.; Besenbacher, F.; Linderoth, T. R. Manuscript submitted.
(51) From left to right: 1,3,5-tris[(5-*tert*-butyl-3-formyl-4-hydroxyphenyl)ethynyl]benzene, and *p*- and *m*-bis[(5-tert-butyl-3-formyl-4-hydroxyphenyl)ethynyl]benzene.
(52) Donhauser, Z. J.; Mantooth, B. A.; Kelly, K. F.; Bumm, L. A.; Monnell, J. D.; Stapelton, J. J.; Price, D. W.; Rawlett, A. M.; Allara, D. L.; Tour, J. M.; Weiss, P. S. *Science* **2001**, *292*, 2303−2307.
(53) Reichert, J.; Ochs, R.; Beckmann, D.; Weber, H. B.; Mayor, M.; von Löhneysen, H. *Phys. Rev. Lett.* **2002**, *88*, 176804.
(54) Suzuki, H.; Miki, H.; Yokoyama, S.; Mashiko, S. *J. Phys. Chem. B* **2003**, *107*, 3662−3689.
(55) Suzuki, H.; Miki, H.; Yokoyama, S.; Mashiko, S. *Thin Solid Films* **2003**, *438*, 97−100.
(56) Bock, C. W.; Hargittai, I. *Struct. Chem.* **1994**, *5*, 307−312.
(57) Berner, S.; Brunner, M.; Ramoino, L.; Suzuki, H.; Güntherodt, H.-J.; Jung, T. A. *Chem. Phys. Lett.* **2001**, *348*, 175−181.
(58) Pascual, J. I.; Barth, J. V.; Ceballos, G.; Trimarchi, G.; DeVita, A.; Kern, K.; Rust, H. P. *J. Chem. Phys.* **2004**, *120*, 11367.
(59) Bombis, Ch.; et al. Manuscript in preparation.